Available online at www.sciencedirect.com
ScienceDirect
Journal of Nuclear Materials 372 (2008) 164–170
journal of nuclear materials
www.elsevier.com/locate/jnucmat

An analytical study on the irradiation-induced stresses in nuclear graphite moderator bricks

Haiyan Li, Alex S.L. Fok *, Barry J. Marsden

School of Mechanical, Aerospace and Civil Engineering, The University of Manchester, Manchester M60 1QD, UK

Received 2 May 2006; accepted 9 March 2007

Abstract

An analytical model for analyzing the stresses of a hypothetical nuclear graphite moderator brick is presented, considering dimensional change and other property changes due to fast neutron irradiation. The relationship between the stresses and the dimensional change of the material was studied, together with the sensitivity of the stresses to other factors such as the brick geometry, irradiation-induced creep, and Poisson's ratio. The analytical results agree well with those predicted by the finite element method. The analytical model can therefore provide a useful means for validating more sophisticated numerical tools and performing quick sensitivity analysis.

1. Introduction

A typical graphite moderated reactor core is constructed from a large number of graphite moderator bricks. Under fast neutron irradiation, the graphite suffers damage to the crystal structure, which causes a change in their physical and mechanical properties such as dimensions, Young's modulus, strength, coefficient of thermal expansion and thermal conductivity. Because of the presence of a dose gradient, and therefore differential dimensional and property changes, internal stresses are generated in the graphite moderator bricks, which are partly relieved by irradiation creep. These irradiation-induced property changes to graphite [1] can significantly influence the stress distributions and geometric sizes of the graphite bricks and, hence, the integrity of the whole reactor structure. Significant deformation or fracture of moderator bricks due to internal and external stresses may impair fuel and control rod movement. Damage to the graphite components may also alter the coolant flow paths. Therefore, it is important to assess the stresses, both internally and externally generated, in the moderator bricks.

Sophisticated numerical models based on the finite element method have been developed by many workers to assess the self-stresses in nuclear graphite components induced by irradiation [2,3]. These numerical models are useful since new components are being designed and the empirical rules used to construct the codes are often revised in view of operational experience and new materials testing data. However, given the complexity of the problems, the performance of such stress analyses requires specialist knowledge and is often time-consuming. It would therefore be advantageous to have an analytical solution, albeit using a simplified geometry, which can capture the essential behaviour of a nuclear graphite component subjected to neutron irradiation. It would also allow sensitivity and parametric studies to be carried out more easily.

In this paper, an analytical study on the stresses is presented for a hollow graphite cylinder undergoing dimensional change and other property changes due to fast neutron irradiation. The sensitivity of the stress magnitude to changes in the rates of dimensional change and irradiation creep was also investigated. The analytical solution should be useful in verifying the numerical solutions obtained from more sophisticated finite element models

* Corresponding author. Tel.: +44 0 161 275 4327; fax: +44 0 161 275 4328.
E-mail address: alex.fok@manchester.ac.uk (A.S.L. Fok).

0022-3115/$ - see front matter © 2007 Elsevier B.V. All rights reserved.
doi:10.1016/j.jnucmat.2007.03.041

and may form the basis for a benchmark test for future stress analysis code development.

2. Geometry and material

The nominal dimensions of the graphite cylinder considered are shown in Fig. 1. The cylinder was assumed to be subjected to a dose profile which decreases linearly in the outward radial direction. The hypothetical irradiation period was 30 years, with the irradiation temperature remaining constant at 500 °C. The dose (EDND) at the end of this period was 200×10^{20} n/cm^2 at the bore and 112×10^{20} n/cm^2 at the outer surface.

The material was assumed to be isotropic and its virgin properties are shown in Table 1. Property changes induced by irradiation, such as those of Young's modulus, strength, coefficient of thermal expansion (CTE), and irradiation creep, etc., are obtained on samples irradiated in material test reactors as a function of fast neutron dose and irradiation temperature [4].

In structural analysis for nuclear graphite moderator bricks, dimensional change is considered to be an irradiation-induced strain that changes with irradiation temperature and irradiation dose. The dimensional change of typical graphite against neutron dose at an irradiation temperature of 500 °C is shown in Fig. 2 [5]. The corresponding rate of change is shown in Fig. 3.

The irradiation creep rule used is [6]

$$\varepsilon^{c} = \varepsilon^{cp} + \varepsilon^{cs}, \tag{1}$$

$$\varepsilon^{cp} = 4.0\exp(-4\gamma)\int_0^{\gamma} \frac{\sigma}{E_c}\exp(4\gamma')\mathrm{d}\gamma', \tag{2}$$

$$\varepsilon^{cs} = 0.23\int_0^{\gamma} \frac{\sigma}{E_c}\mathrm{d}\gamma', \tag{3}$$

where ε^{c} is the total creep strain, ε^{cp} is the primary creep strain, ε^{cs} is the secondary creep strain, E_c is the creep modulus as discussed in Ref. [1], σ is the stress, and γ is the fast neutron dose (10^{20} n/cm^2 EDND).

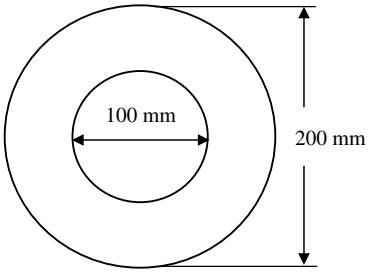

Fig. 1. Geometry of a generic graphite moderator brick.

Table 1
Virgin graphite properties

Young's modulus (GPa)	10.0
Poisson's ratio	0.2
Coefficient of thermal expansion (10^{-6}/°C)	4.39

Fig. 4 shows the dynamic and creep Young's modulus of the graphite as functions of dose. Poisson's ratio was assumed to remain a constant of 0.2. For simplicity, thermal strains were ignored. The change of CTE with dose was therefore not considered in this analytical analysis.

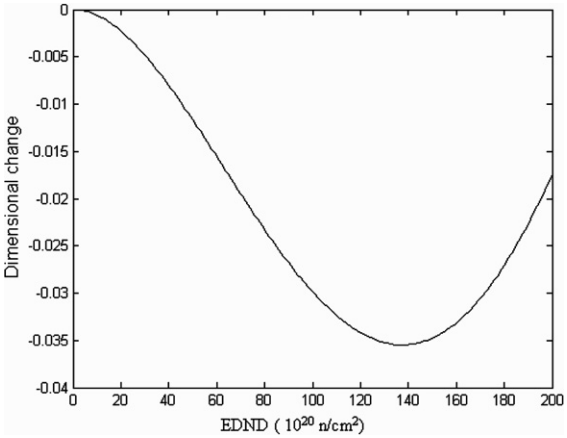

Fig. 2. Dimensional change of graphite vs. dose.

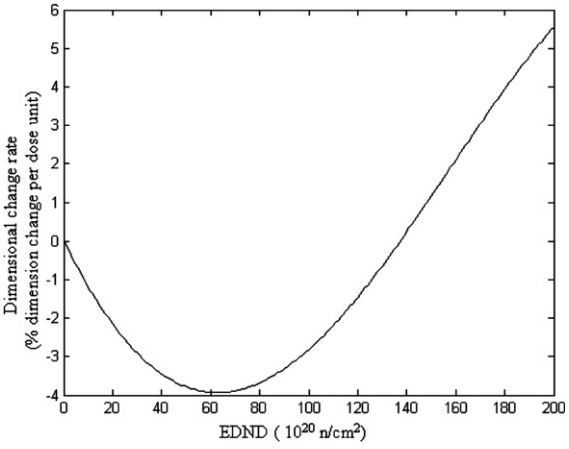

Fig. 3. Dimensional change rate of graphite vs. dose.

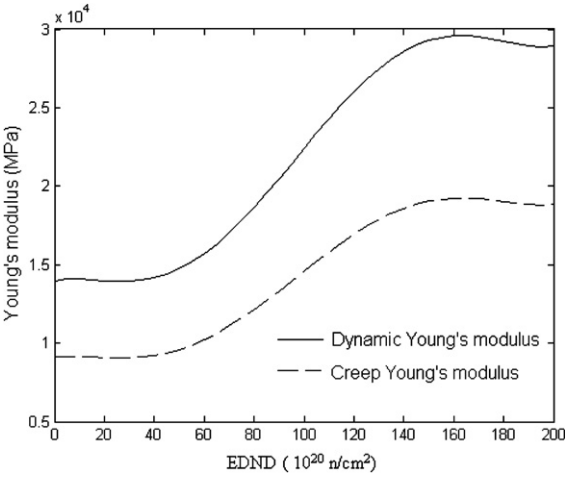

Fig. 4. Dynamic and creep Young's moduli vs. dose.

3. Theory

The following analysis is based on that due to Cornwall [7] developed in the 1960s. The relevant UKAEA report is available from the UK Public Records Office. It also extends the work of the authors for the case of plane stress which was reported in Ref. [8].

The moderator brick is treated as a very long hollow cylinder in which rotational symmetry is assumed. Ignoring thermal strain, the stress–strain equations, including the elastic strains, creep strains and dimensional change strain, in cylindrical co-ordinates, are

$$\varepsilon_{rr} = \frac{1}{E}(\sigma_{rr} - \nu\sigma_{\theta\theta} - \nu\sigma_{zz}) + \varepsilon^{c}_{rr} + \varepsilon^{d}, \tag{4}$$

$$\varepsilon_{\theta\theta} = \frac{1}{E}(\sigma_{\theta\theta} - \nu\sigma_{rr} - \nu\sigma_{zz}) + \varepsilon^{c}_{\theta\theta} + \varepsilon^{d}, \tag{5}$$

$$\varepsilon_{zz} = \frac{1}{E}(\sigma_{zz} - \nu\sigma_{rr} - \nu\sigma_{\theta\theta}) + \varepsilon^{c}_{zz} + \varepsilon^{d}, \tag{6}$$

where ε_{ii} $(i = r, \theta, z)$ are total strains, σ_{ii} are direct stresses, ε^{c}_{ii} are creep strains, ε^{d} is the dimensional change strain which is the same in all directions since isotropic properties are assumed, E is Young's modulus and ν is Poisson's ratio. No summation is implied by the double subscript notation.

For simplicity, primary creep strains (which are small compared to secondary creep strains at moderate to high doses) are ignored and only secondary creep strains are considered, i.e.

$$\varepsilon^{c}_{rr} = 0.23\int_0^{\gamma}\frac{(\sigma_{rr} - \nu_c\sigma_{\theta\theta} - \nu_c\sigma_{zz})}{E_c}\mathrm{d}\gamma', \tag{7}$$

$$\varepsilon^{c}_{\theta\theta} = 0.23\int_0^{\gamma}\frac{(\sigma_{\theta\theta} - \nu_c\sigma_{rr} - \nu_c\sigma_{zz})}{E_c}\mathrm{d}\gamma', \tag{8}$$

$$\varepsilon^{c}_{zz} = 0.23\int_0^{\gamma}\frac{(\sigma_{zz} - \nu_c\sigma_{\theta\theta} - \nu_c\sigma_{rr})}{E_c}\mathrm{d}\gamma', \tag{9}$$

where E_c and ν_c are Young's modulus and Poisson's ratio for irradiation creep. For simplicity, it is assumed that $\nu_c = \nu$.

Referring to Fig. 2, the dimensional change strain, ε^{d}, is expressed as a function of fast neutron dose γ using a 5th degree polynomial as

$$\varepsilon^{d} = A_0\gamma^5 + A_1\gamma^4 + A_2\gamma^3 + A_3\gamma^2 + A_4\gamma + A_5, \tag{10}$$

where $A_0, A_1, \ldots$, etc. are coefficients derived from the polynomial fit (Table 2). Similarly, the dynamic and creep Young's modulus, E and E_c (Fig. 4), can be expressed as

$$E = B_0\gamma^5 + B_1\gamma^4 + B_2\gamma^3 + B_3\gamma^2 + B_4\gamma + B_5, \tag{11}$$

$$E_c = C_0\gamma^5 + C_1\gamma^4 + C_2\gamma^3 + C_3\gamma^2 + C_4\gamma + C_5, \tag{12}$$

where $B_0, B_1, \ldots$ and $C_0, C_1, \ldots$, etc. are coefficients derived from the respective polynomial fits (Table 2).

Substituting Eqs. (7)–(9) into the stress–strain equations of (4)–(6) gives

$$E\varepsilon_{rr} = (\sigma_{rr} - \nu\sigma_{\theta\theta} - \nu\sigma_{zz}) + 0.23E\int_0^{\gamma}\frac{(\sigma_{rr} - \nu\sigma_{\theta\theta} - \nu\sigma_{zz})}{E_c}\mathrm{d}\gamma' + E\varepsilon^{d}, \tag{13}$$

$$E\varepsilon_{\theta\theta} = (\sigma_{\theta\theta} - \nu\sigma_{rr} - \nu\sigma_{zz}) + 0.23E\int_0^{\gamma}\frac{(\sigma_{\theta\theta} - \nu\sigma_{rr} - \nu\sigma_{zz})}{E_c}\mathrm{d}\gamma' + E\varepsilon^{d}, \tag{14}$$

$$E\varepsilon_{zz} = (\sigma_{zz} - \nu\sigma_{\theta\theta} - \nu\sigma_{rr}) + 0.23E\int_0^{\gamma}\frac{(\sigma_{zz} - \nu\sigma_{\theta\theta} - \nu\sigma_{rr})}{E_c}\mathrm{d}\gamma' + E\varepsilon^{d}. \tag{15}$$

Differentiating the above equations with respect to dose then gives

$$E\dot{\varepsilon}_{rr} = (\dot{\sigma}_{rr} - \nu\dot{\sigma}_{\theta\theta} - \nu\dot{\sigma}_{zz}) + 0.23E\frac{(\sigma_{rr} - \nu\sigma_{\theta\theta} - \nu\sigma_{zz})}{E_c} + E\dot{\varepsilon}^{d}, \tag{16}$$

$$E\dot{\varepsilon}_{\theta\theta} = (\dot{\sigma}_{\theta\theta} - \nu\dot{\sigma}_{rr} - \nu\dot{\sigma}_{zz}) + 0.23E\frac{(\sigma_{\theta\theta} - \nu\sigma_{rr} - \nu\sigma_{zz})}{E_c} + E\dot{\varepsilon}^{d}, \tag{17}$$

$$E\dot{\varepsilon}_{zz} = (\dot{\sigma}_{zz} - \nu\dot{\sigma}_{\theta\theta} - \nu\dot{\sigma}_{rr}) + 0.23E\frac{(\sigma_{zz} - \nu\sigma_{\theta\theta} - \nu\sigma_{rr})}{E_c} + E\dot{\varepsilon}^{d}, \tag{18}$$

where $\dot{\varepsilon} = \frac{\partial}{\partial\gamma}(\varepsilon)$, and γ is taken to be a function of time t and radial position r in the form of

$$\gamma = (k_0 + k_1 r)\cdot t. \tag{19}$$

Note that, for simplicity, the rate of change of Young's modulus with dose, $\dot{E}$, is ignored. This is justified because the products $\dot{E}\varepsilon$ are much smaller than $E\dot{\varepsilon}$ throughout the irradiation period.

To determine the stress distribution within the graphite cylinder, the equilibrium equation must be solved in conjunction with the compatibility and constitutive equations. Using the Laplace transformation, these equations can be simplified to contain terms of the independent variable r only, as in classical elasticity theory. Then, through inverse transformation the variable γ can be recovered. The

Table 2
Polynomial coefficients for dimensional change (A), dynamic Young's modulus (B) and creep Young's modulus (C)

Coefficient	A_0	A_1	A_2	A_3	A_4	A_5
Value	−1.043E−13	−2.10E−11	3.923E−8	−6.629E−6	3.355E−6	0.0
Coefficient	B_0	B_1	B_2	B_3	B_4	B_5
Value	9.397E−7	−4.610E−4	6.923E−2	−2.6907	2.793E1	1.399E4
Coefficient	C_0	C_1	C_2	C_3	C_4	C_5
Value	6.114E−7	−2.999E−4	4.504E−2	−1.7506	1.817E1	9.1029E3

detailed derivation is shown in Appendix A, with the stress components obtained being

$$\sigma_{rr} = \frac{E}{(1-v)} e^{[(-0.23E/E_c)\gamma]} \int_0^{g=\gamma} e^{(0.23E/E_c)g} d[\varsigma_1(g)], \quad (20)$$

$$\sigma_{\theta\theta} = \frac{E}{(1-v)} e^{[(-0.23E/E_c)\gamma]} \int_0^{g=\gamma} e^{(0.23E/E_c)g} d[\varsigma_2(g)], \quad (21)$$

$$\sigma_{zz} = \frac{E}{(1-v)} e^{[(-0.23E/E_c)\gamma]} \int_0^{g=\gamma} e^{(0.23E/E_c)g} d[\varsigma_3(g)], \quad (22)$$

where

$$\varsigma_1 = \frac{1}{r^2}\frac{r^2-a^2}{b^2-a^2}\int_a^b \varepsilon^d r\,dr - \frac{1}{r^2}\int_a^r \varepsilon^d r\,dr, \quad (23)$$

$$\varsigma_2 = \frac{1}{r^2}\frac{r^2+a^2}{b^2-a^2}\int_a^b \varepsilon^d r\,dr + \frac{1}{r^2}\int_a^r \varepsilon^d r\,dr - \varepsilon^d, \quad (24)$$

$$\varsigma_3 = \frac{2}{b^2-a^2}\int_a^b \varepsilon^d r\,dr - \varepsilon^d, \quad (25)$$

a and b being the inner and outer radii of the cylinder.

4. Results and discussion

The technical computing language software Matlab [10] was used to perform the numerical integration in calculating the stresses of Eqs. (20)–(22).

Figs. 5–7 give the analytical results of the hoop, axial and radial stresses at the inner and outer surfaces of the cylinder. The hoop and axial stresses have a similar profile and time history, being tensile at the bore and compressive at the outer surface in the first half of the irradiation period and then reversing in sign in the second half. The radial stress is negligible throughout.

The corresponding 3-D finite element (FE) results for the mid-height position of a rectangular brick with a square cross-section having a bore hole of the same diameter [5] are also plotted in Figs. 5–7 for comparison. It can be seen that the analytical results are in good agreement with the FE results, especially in early life. The discrepancy between the analytical and FE results can be attributed to differences in geometries, input material curves and the boundary conditions assumed. Also, in the analytical solution, the differentials of the Young's and creep moduli with respect to dose are ignored, even though they are functions of dose. Note that the analytical solution will not be applicable to the ends of the cylinder where plane-stress conditions hold.

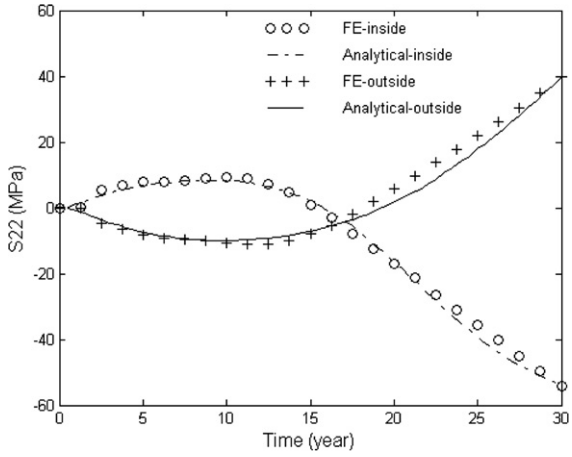

Fig. 5. Time histories of hoop stresses at the bore and outer surface of the cylinder.

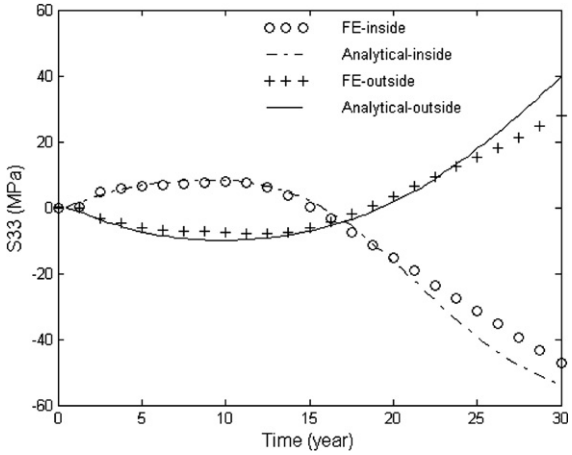

Fig. 6. Time histories of axial stresses at the bore and outer surface of the cylinder.

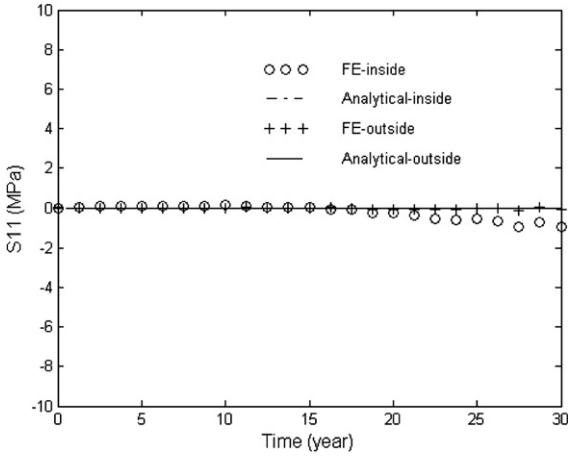

Fig. 7. Time histories of radial stresses at the bore and outer surface of the cylinder.

By comparing Figs. 5 and 6 with Fig. 3, it can be seen that the turnaround of the stresses appear to be directly related to that of the dimensional change rate at the bore. To verify the possible relationship between the stresses and dimensional change rate, different dimensional change rate curves (Fig. 8) were used to calculate the stresses. The corresponding hoop stresses are shown in Fig. 9. It can be seen that the turnaround of hoop stresses of the brick are closely related to that of the dimensional change rate at the bore of the brick, delaying the turnaround of the latter will lead to a corresponding delay in the former.

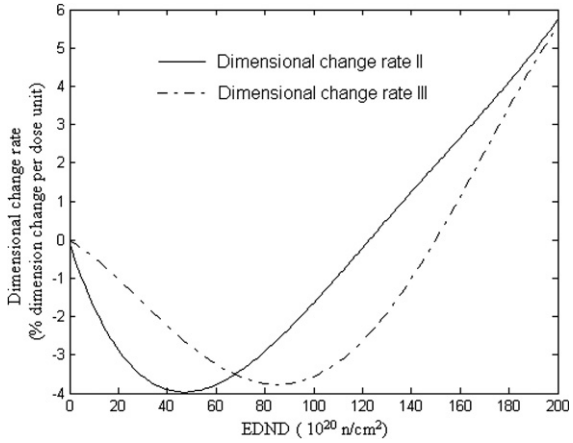

Fig. 8. Dimensional change rates II and III used in sensitivity study.

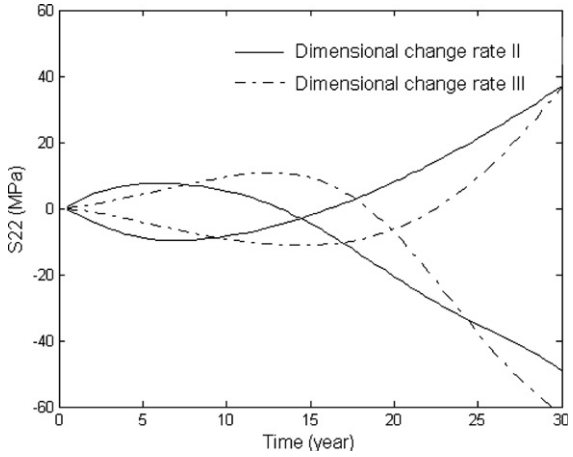

Fig. 9. Hoop stresses vs. time using different dimensional change rates (II and III).

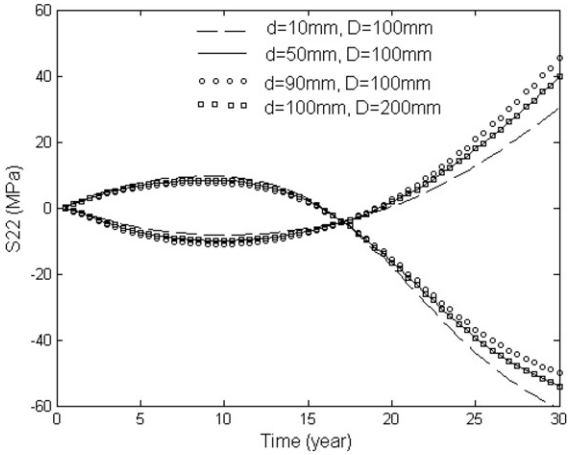

Fig. 10. Hoop stresses vs. time with different inner (d) and outer (D) diameters.

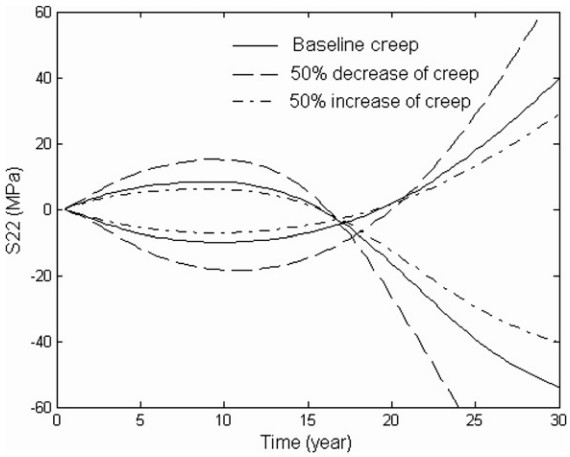

Fig. 11. Hoop stresses vs. time with different levels of creep.

Graphite cylinders with different geometries were also analyzed to verify this relationship. Fig. 10 shows the hoop stresses with different inner and outer diameters. It shows that the turnaround of the hoop stresses depends only on that of the dimensional change rate, and not on the geometry. The stress value is more sensitive to the outer to inner diameter ratio, though. Increasing the outer to inner diameter ratio will increase the ratio of the outer to inner hoop stress ratio, and vice versa. This has been confirmed by further calculations.

To investigate the effect of irradiation-induced creep on the stresses, calculations have been performed with both a decrease and increase in the creep level. Fig. 11 shows the hoop stresses with different amounts of creep: 50% decrease and 50% increase from the value used in previous calculations. It shows that irradiation-induced creep has an important effect on the stress level. For this particular model, decreasing creep by 50% increases the peak value of the hoop stress at turnaround by 50%. Conversely, increasing creep by 50% reduces the peak value of the hoop stress by about 30%.

For simplicity, the elastic and creep Poisson's ratios were assumed to be the same ($v = v_c = 0.2$). The influence of Poisson's ratio on the results was also studied. Fig. 12 illustrates the difference in the hoop stress when using

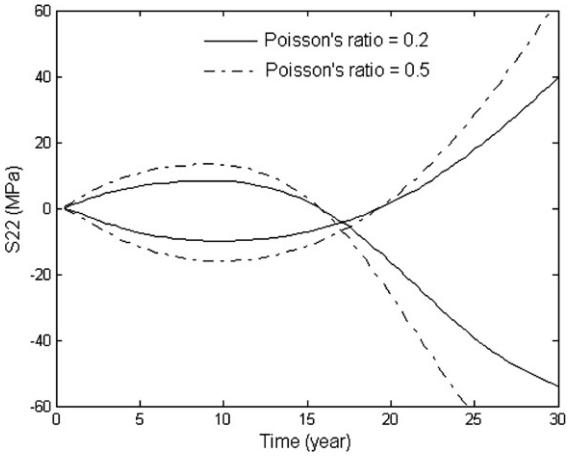

Fig. 12. Hoop stresses vs. time with different Poisson's ratios.

different Poisson's ratios. It shows that an increase of Poisson's ratio will increase the stress levels but it will not change the time of turnaround of the stresses. When Poisson's ratio changes from 0.2 to 0.5, the stress magnitudes at turnaround will increase by more than 50%.

5. Conclusions

An analytical model has been developed to analyze the self-stresses in nuclear graphite cylindrical bricks undergoing irradiation-induced dimensional and property changes. The analytical stress results show good agreement with FE results reported elsewhere for a similar geometry.

The axial stress is of a similar order to the hoop stress, and they have the same trends with irradiation dose as well. Both axial and hoop stresses at the bore are tensile in the first half of the irradiation period and become compressive in the second half. The reverse is true for these stresses at the outer surface of the brick. The radial stress is negligibly small.

The dimensional change rate at the brick bore has a close relationship with the hoop stress history. The time of turnaround of the hoop stresses follows closely that of the dimensional change rate at the bore of the brick. This is true irrespective of the outer to inner diameter ratio of the brick. However, the magnitude of the stresses is more sensitive to the diameter ratio: the larger the outer to inner diameter ratio, the larger the ratio between the stresses at the outside of the brick and those at the bore.

The stresses are very sensitive to the level of irradiation-induced creep. A 50% decrease of creep can result in a 50% increase of hoop stresses, while a 50% increase of creep can result in a 30% decrease of hoop stresses.

The stresses are also significantly influenced by the value of Poisson's ratio. An increase of Poisson's ratio will increase the values of stresses, but it will not change the time of the turnaround of the stress. When Poisson's ratio increases from 0.2 to 0.5, the stress magnitudes at turnaround will increase by more than 50%.

Appendix I. Derivation of irradiation-induced stresses via Laplace transformation

The Laplace transformation of a function $f(r,\gamma)$ is defined as

$$\bar{f}(r,s)=\int_0^\infty \mathrm{e}^{-s\gamma}f(r,\gamma)\mathrm{d}\gamma. \tag{A.1}$$

Thus, transforming Eqs. (16)–(18), and noting that the stresses and strains are zero at $\gamma=0$, gives

$$sE\bar{\varepsilon}_{rr}=s(\bar{\sigma}_{rr}-v\bar{\sigma}_{\theta\theta}-v\bar{\sigma}_{zz})+0.23E\frac{(\bar{\sigma}_{rr}-v\bar{\sigma}_{\theta\theta}-v\bar{\sigma}_{zz})}{E_c}+sE\bar{\varepsilon}^{d}, \tag{A.2}$$

$$sE\bar{\varepsilon}_{\theta\theta}=s(\bar{\sigma}_{\theta\theta}-v\bar{\sigma}_{rr}-v\bar{\sigma}_{zz})+0.23E\frac{(\bar{\sigma}_{\theta\theta}-v\bar{\sigma}_{rr}-v\bar{\sigma}_{zz})}{E_c}+sE\bar{\varepsilon}^{d}, \tag{A.3}$$

$$sE\bar{\varepsilon}_{zz}=s(\bar{\sigma}_{zz}-v\bar{\sigma}_{\theta\theta}-v\bar{\sigma}_{rr})+0.23E\frac{(\bar{\sigma}_{zz}-v\bar{\sigma}_{\theta\theta}-v\bar{\sigma}_{rr})}{E_c}+sE\bar{\varepsilon}^{d}. \tag{A.4}$$

To simplify the analysis, it is supposed that the cylinder is constrained longitudinally so that $\partial\varepsilon_{zz}/\partial r=0$. Hence, $\varepsilon_{zz}=\varphi(\gamma)$ and

$$\bar{\varepsilon}_{zz}=\bar{\varphi}(s). \tag{A.5}$$

From (A.4) and (A.5),

$$\bar{\sigma}_{zz}=v(\bar{\sigma}_{rr}+\bar{\sigma}_{\theta\theta})+T(\bar{\varphi}(s)-\bar{\varepsilon}^{d}), \tag{A.6}$$

where

$$T=\frac{sE}{s+0.23E/E_c}. \tag{A.7}$$

Then, substituting (A.6) into (A.2) and (A.3) gives

$$\bar{\sigma}_{rr}=\frac{T[(1-v)\bar{\varepsilon}_{rr}+v\bar{\varepsilon}_{\theta\theta}+v\bar{\varphi}(s)-(1+v)\bar{\varepsilon}^{d}]}{1-v-2v^2}, \tag{A.8}$$

$$\bar{\sigma}_{\theta\theta}=\frac{T[(1-v)\bar{\varepsilon}_{\theta\theta}+v\bar{\varepsilon}_{rr}+v\bar{\varphi}(s)-(1+v)\bar{\varepsilon}^{d}]}{1-v-2v^2}. \tag{A.9}$$

The transformed equilibrium equation of the rotationally symmetric brick is

$$\frac{\partial\bar{\sigma}_{rr}}{\partial r}+\frac{\bar{\sigma}_{rr}-\bar{\sigma}_{\theta\theta}}{r}=0. \tag{A.10}$$

Substituting Eqs. (A.8) and (A.9) into (A.10) gives

$$(1-v)\frac{\partial\bar{\varepsilon}_{rr}}{\partial r}+v\frac{\partial\bar{\varepsilon}_{\theta\theta}}{\partial r}+\frac{(1-2v)}{r}(\bar{\varepsilon}_{rr}-\bar{\varepsilon}_{\theta\theta})=(1+v)\frac{\partial\bar{\varepsilon}^{d}}{\partial r}. \tag{A.11}$$

The transformed geometrical equations are

$$\bar{\varepsilon}_{rr}=\frac{\partial\bar{u}}{\partial r}, \tag{A.12}$$

$$\bar{\varepsilon}_{\theta\theta}=\frac{\bar{u}}{r}, \tag{A.13}$$

from which the following transformed compatibility equation can be derived:

$$\frac{\partial\bar{\varepsilon}_{\theta\theta}}{\partial r}=\frac{\bar{\varepsilon}_{rr}-\bar{\varepsilon}_{\theta\theta}}{r}. \tag{A.14}$$

Eq. (A.11) can then be rewritten as

$$\frac{\partial(\bar{\varepsilon}_{rr}+\bar{\varepsilon}_{\theta\theta})}{\partial r}=\left(\frac{1+v}{1-v}\right)\frac{\partial\bar{\varepsilon}^{d}}{\partial r} \tag{A.15}$$

or

$$\frac{\partial}{\partial r}\left(\frac{1}{r}\frac{\partial}{\partial r}(r\bar{u})\right)=\left(\frac{1+v}{1-v}\right)\frac{\partial\bar{\varepsilon}^{d}}{\partial r}. \tag{A.16}$$

Integrating between the limits r and a, the inner radius, gives

$$\bar{u}=\frac{1+v}{r(1-v)}\left\{\int_a^r\bar{\varepsilon}^{d}r\,\mathrm{d}r\right\}+Cr+\frac{D}{r}, \tag{A.17}$$

where C and D are integral constants.

Then from Eqs. (A.8), (A.9), (A.12) and (A.13), $\bar{\sigma}_{rr}$ and $\bar{\sigma}_{\theta\theta}$ can be determined as

$$\bar{\sigma}_{rr} = -\frac{T}{r^2(1-v)}\left\{\int_a^r \bar{\varepsilon}^{\mathrm{d}} r\,\mathrm{d}r\right\} + M + \frac{N}{r^2}, \tag{A.18}$$

$$\bar{\sigma}_{\theta\theta} = \frac{T}{r^2(1-v)}\left\{\int_a^r \bar{\varepsilon}^{\mathrm{d}} r\,\mathrm{d}r - \bar{\varepsilon}^{\mathrm{d}} r^2\right\} + M - \frac{N}{r^2}, \tag{A.19}$$

where M and N are also integral constants to be determined by the boundary conditions.

The boundary conditions at the inner (a) and outer radius (b), i.e. $\sigma_{rr} = 0$ at $r = a$ and $r = b$, give

$$\bar{\sigma}_{rr} = 0 \text{ at } r = a \quad \text{and } r = b. \tag{A.20}$$

Thus,

$$M = -\frac{T}{(a^2-b^2)(1-v)}\left\{\int_a^b \bar{\varepsilon}^{\mathrm{d}} r\,\mathrm{d}r\right\}, \tag{A.21}$$

$$N = \frac{a^2 T}{(a^2-b^2)(1-v)}\left\{\int_a^b \bar{\varepsilon}^{\mathrm{d}} r\,\mathrm{d}r\right\} \tag{A.22}$$

and it follows that:

$$\bar{\sigma}_{rr} = \frac{T}{r^2(1-v)}\left\{\frac{r^2-a^2}{b^2-a^2}\int_a^b \bar{\varepsilon}^{\mathrm{d}} r\,\mathrm{d}r - \int_a^r \bar{\varepsilon}^{\mathrm{d}} r\,\mathrm{d}r\right\}, \tag{A.23}$$

$$\bar{\sigma}_{\theta\theta} = \frac{T}{r^2(1-v)}\left\{\frac{r^2+a^2}{b^2-a^2}\int_a^b \bar{\varepsilon}^{\mathrm{d}} r\,\mathrm{d}r + \int_a^r \bar{\varepsilon}^{\mathrm{d}} r\,\mathrm{d}r - \bar{\varepsilon}^{\mathrm{d}} r^2\right\}. \tag{A.24}$$

To find $\bar{\sigma}_{zz}$, the function $\bar{\varphi}(s)$ must be determined. Substituting Eqs. (A.18) and (A.19) into Eq. (A.6) gives

$$\bar{\sigma}_{zz} = -\frac{T\bar{\varepsilon}^{\mathrm{d}}}{(1-v)} + (2vM + T\bar{\varphi}(s)). \tag{A.25}$$

Invoking the equilibrium condition in the z-direction, i.e.

$$\int_a^b \bar{\sigma}_{zz} r\,\mathrm{d}r = 0, \tag{A.26}$$

then gives

$$\bar{\varphi}(s) = \frac{1}{(1-v)}\left\{\frac{2}{b^2-a^2}\int_a^b \bar{\varepsilon}^{\mathrm{d}} r\,\mathrm{d}r\right\} - \frac{2vM}{T}, \tag{A.27}$$

$$\bar{\sigma}_{zz} = \frac{T}{(1-v)}\left\{\frac{2}{b^2-a^2}\int_a^b \bar{\varepsilon}^{\mathrm{d}} r\,\mathrm{d}r - \bar{\varepsilon}^{\mathrm{d}}\right\}. \tag{A.28}$$

Replacing T with $\frac{sE}{s+0.23E/E_{\mathrm{c}}}$, Eqs. (A.23), (A.24) and (A.28) can be rewritten as

$$\bar{\sigma}_{rr} = \frac{E}{(1-v)}\frac{s}{(s+0.23E/E_{\mathrm{c}})}\frac{1}{r^2} \times \left\{\frac{r^2-a^2}{b^2-a^2}\int_a^b \bar{\varepsilon}^{\mathrm{d}} r\,\mathrm{d}r - \int_a^r \bar{\varepsilon}^{\mathrm{d}} r\,\mathrm{d}r\right\}, \tag{A.29}$$

$$\bar{\sigma}_{\theta\theta} = \frac{E}{(1-v)}\frac{s}{(s+0.23E/E_{\mathrm{c}})}\frac{1}{r^2} \times \left\{\frac{r^2+a^2}{b^2-a^2}\int_a^b \bar{\varepsilon}^{\mathrm{d}} r\,\mathrm{d}r + \int_a^r \bar{\varepsilon}^{\mathrm{d}} r\,\mathrm{d}r - \bar{\varepsilon}^{\mathrm{d}} r^2\right\}, \tag{A.30}$$

$$\bar{\sigma}_{zz} = \frac{E}{(1-v)}\frac{s}{(s+0.23E/E_{\mathrm{c}})} \times \left\{\frac{2}{b^2-a^2}\int_a^b \bar{\varepsilon}^{\mathrm{d}} r\,\mathrm{d}r - \bar{\varepsilon}^{\mathrm{d}}\right\}. \tag{A.31}$$

Finally, Eqs. (A.29), (A.30) and (A.31) can be inverted using Duhamel's formula for the convolution principle [9]:

$$[F(s)][s\bar{\varsigma}(s)] = \int_0^\infty \left\{f(\gamma)\varsigma(0) + \int_0^\gamma f(\gamma-g)\frac{\partial}{\partial g}[\varsigma(g)]\mathrm{d}g\right\} \times \exp(-s\gamma)\mathrm{d}\gamma, \tag{A.32}$$

where $F(s)$ and $[s\bar{\varsigma}(s)]$ are Laplace transforms of $f(\gamma)$ and $\frac{\partial}{\partial g}[\varsigma(g)]$, respectively.

Here, $F(s) = \frac{1}{s+0.23E/E_{\mathrm{c}}}$, so $f(\gamma) = \exp[-(0.23E/E_{\mathrm{c}})\gamma]$, and

$$\varsigma_1 = \frac{1}{r^2}\frac{r^2-a^2}{b^2-a^2}\int_a^b \varepsilon^{\mathrm{d}} r\,\mathrm{d}r - \frac{1}{r^2}\int_a^r \varepsilon^{\mathrm{d}} r\,\mathrm{d}r, \tag{A.33}$$

$$\varsigma_2 = \frac{1}{r^2}\frac{r^2+a^2}{b^2-a^2}\int_a^b \varepsilon^{\mathrm{d}} r\,\mathrm{d}r + \frac{1}{r^2}\int_a^r \varepsilon^{\mathrm{d}} r\,\mathrm{d}r - \varepsilon^{\mathrm{d}}, \tag{A.34}$$

$$\varsigma_3 = \frac{2}{b^2-a^2}\int_a^b \varepsilon^{\mathrm{d}} r\,\mathrm{d}r - \varepsilon^{\mathrm{d}}. \tag{A.35}$$

Noting that $\varsigma_i(0) = 0$ at $\gamma = 0$, the inversion gives

$$\sigma_{rr} = \frac{E}{(1-v)}\mathrm{e}^{[(-0.23E/E_{\mathrm{c}})\gamma]}\int_0^{g=\gamma}\mathrm{e}^{(0.23E/E_{\mathrm{c}})g}\mathrm{d}[\varsigma_1(g)], \tag{A.36}$$

$$\sigma_{\theta\theta} = \frac{E}{(1-v)}\mathrm{e}^{[(-0.23E/E_{\mathrm{c}})\gamma]}\int_0^{g=\gamma}\mathrm{e}^{(0.23E/E_{\mathrm{c}})g}\mathrm{d}[\varsigma_2(g)], \tag{A.37}$$

$$\sigma_{zz} = \frac{E}{(1-v)}\mathrm{e}^{[(-0.23E/E_{\mathrm{c}})\gamma]}\int_0^{g=\gamma}\mathrm{e}^{(0.23E/E_{\mathrm{c}})g}\mathrm{d}[\varsigma_3(g)]. \tag{A.38}$$

References

[1] B.J. Marsden, Graphite for High-Temperature Reactors, EPRI, Palo Alto, CA, 2001, p. 1003013.
[2] M. Ishihara, T. Iyoku, S. Shiozawa, H. Shirai, N. Takikawa, in: Transactions of the 12th International Conference on Structural Mechanics in Reactor Technology, 1993, p. 167.
[3] Z. Zhang, J. Guo, L. Ma, Y. Zhou, M. Ying, Hedongli Gongcheng/ Nucl. Power Eng. 17 (3) (1996) 250 (Language: Chinese).
[4] J.E. Brocklehurst, B.T. Kelly, Carbon 31 (1993) 155.
[5] H. Li, B.J. Marsden, S.L. Fok, Nucl. Eng. Des. 232 (2004) 237.
[6] B.T. Kelly, J.E. Brocklehurst, J. Nucl. Mater. 65 (1977) 79.
[7] W.S. Cornwall, Wigner Stresses. United Kingdom Atomic Energy Authority, TRG Report 40(R), 1962 (Available from the UK Public Records Office).
[8] H. Li, B.J. Marsden, S.L. Fok, in: 18th International Conference on Structural Mechanics in Reactor Technology (Smirt-18), Beijing, August 2005.
[9] P.I. Romanovskii, Mathematical Methods for Engineers and Technologists, Pergamon, Oxford, 1961.
[10] Hanselman, Duane C. Mastering MATLAB 6. 2001.